IEEJ Journal of Industry Applications
Vol.7 No.1 pp.1–14 DOI: 10.1541/ieejjia.7.1

Review Paper

Disturbance Observer and Kalman Filter Based Motion Control Realization

Thao Tran Phuong[*a)] Member, Kiyoshi Ohishi[*] Fellow
Chowarit Mitsantisuk[**] Member, Yuki Yokokura[*] Member
Kouhei Ohnishi[***] Fellow, Roberto Oboe[****] Member
Asif Sabanovic[*5] Non-member

(Manuscript received Oct. 23, 2017, revised Nov. 7, 2017)

Many effective robot-manipulator control schemes using a disturbance observer have been reported in the literature in the past decades. Besides, the disturbance observer combined with the Kalman filter has attracted the attention of researchers in the field of motion control. The major advantage of a motion control system based on the Kalman filter and disturbance observer is the realization of high robustness against disturbance and parameter variations, effective noise suppression and wideband force sensing. This paper presents a survey of motion control based on the Kalman filter and disturbance observer, which have been previously introduced by the authors. Several control schemes, as well as formulations and applications of the Kalman filter and disturbance observer, are described in the paper. The performance and effectiveness of the control schemes are evaluated to give a useful and comprehensive design of the Kalman filter and disturbance observer in various motion control applications.

Keywords: disturbance observer, Kalman filter, motion control, acceleration control, force control, real-world haptics

1. Introduction

For several decades, motion control using disturbance observer (DOB) has been extensively reported in the literature and employed for various applications for the control of industrial robotics, human-robot interaction, machine tools, bilateral control, motion copying system and robotic surgery [(1)–(5)]. Conventionally, in a force control system, force measurement is realized using force sensors. Although commercial force sensors benefit from their accuracy, flexibility, and reliability, the use of force sensors in a force control system has its own noteworthy downsides. Most force sensors are not very durable and are vulnerable to impact. Besides, high-precision force sensors are not economical for limited budget projects. Moreover, force sensors are susceptible to noise effect, which results in a narrow force-sensing bandwidth, and are not suitable for diverse environments or applications. These drawbacks limit the use of force sensors. Therefore, many approaches have been proposed to develop suitable force observers. One popular force-sensor-less observer method is the disturbance observer [(6)–(8)]. Essentially, the DOB is used instead of a force sensor to estimate and compensate for disturbance. Since its invention, it has become one of the most preferred solutions in motion control. By using the DOB, the disturbance force is rejected, and robust motion control is attained. In fact, the performance of a force control system is determined by the fidelity of force detection. This leads to a large number of elegant approaches to develop the DOB as well as to improve its performance. Xiong and Saif have proposed a state functional disturbance observer to estimate disturbances with a bounded error [(9)]. In this method, the disturbance observer state does not precisely track the system states, which is an advantage that simplifies the estimation error dynamics. To provide satisfactory control performance, Chen et al. have proposed a new nonlinear disturbance observer scheme and applied it to a robotic system [(10)]. Natori et al. have introduced a time delay compensation method based on the concept of network disturbance and communication disturbance observer for network-based control systems [(11)]. A generalized disturbance observer has been proposed by Kim et al. to estimate higher order disturbances in the time series expansion [(12)]. Oh and Kong have proposed the disturbance observer and feed-forward controller as the model-based control algorithm to achieve the high-precision force control of a series elastic actuator [(13)].

Although the DOB has superior performance in terms of robustness, its force sensing performance deteriorates with noise. The effect of noise limits the force sensing bandwidth and causes oscillations in control systems. Recently, the Kalman filter, a powerful tool for estimating the state of a process by minimizing the mean of the squared error, has been widely used in motion control applications [(14)–(26)]. The noise of the measurement system and the estimations is

a) Correspondence to: Thao Tran Phuong. E-mail: thaotp@vos.nagaokaut.ac.jp
* Nagaoka University of Technology
1603-1, Kamitomioka, Nagaoka, Niigata 940-2188, Japan
** Kasetsart University
Thailand
*** Keio University
3-14-1, Hiyoshi, Kohoku-ku, Yokohamak, Kanagawa 223-8522, Japan
**** University of Padova
Italy
*5 International University of Sarajevo
Bosnia and Herzegovina

reduced effectively using the Kalman filter. Therefore, the approach of combining the DOB and Kalman filter in motion control systems has risen to prominence due to its advantages in achieving high robustness against disturbance and parameter variations, effective noise suppression and wideband force sensing.

This paper presents a survey on motion control based on the Kalman filter and the DOB, introduced by the authors in previous works. Several control schemes, as well as formulations and applications of the Kalman filter and the DOB are described in the paper. The performance and effectiveness of the control schemes are evaluated to develop a useful and comprehensive design of the Kalman filter and the DOB in various motion control applications.

The content of the paper is organized as follows: Section 2 gives a description of the Kalman filtering algorithm. Section 3 presents the force-sensor-less observer approaches proposed in our previous works. These observers are designed for disturbance torque or load torque estimation, and are combined with the Kalman filter in motion control schemes. Section 4 introduces the methods to integrate the Kalman filter and the DOB in specific applications of motion control. Section 5 presents the summary and conclusions of the paper.

2. Kalman Filtering Algorithm

The Kalman filter [27] is an optimal estimator that minimizes the mean of the squared error to obtain approximations of the true response using information from a model and available measurements. The Kalman filter estimates the state of a measuring process formulated in the following equations.

$$x_{(k+1)} = \boldsymbol{A}x_{(k)} + \boldsymbol{B}u_{(k)} + w_{(k)} \cdots\cdots (1)$$

$$z_{(k)} = \boldsymbol{H}x_{(k)} + v_{(k)} \cdots\cdots (2)$$

Here, $x_{(k)}$ is the state; $z_{(k)}$ is the measured data corrupted by noise; and $u_{(k)}$ is the known input to the system. The random variables $w_{(k)}$ and $v_{(k)}$ represent the process noise and measurement noise, respectively. k is the sampling time index corresponding to each sampling step of the discrete measuring process. $\boldsymbol{A}$, $\boldsymbol{B}$ and $\boldsymbol{H}$ are the state, control input and observation matrices, respectively.

In (1) and (2), both $w_{(k)}$ and $v_{(k)}$ are assumed to be uncorrelated zero-mean Gaussian white noise with the covariance matrix of process noise, $\boldsymbol{Q}$, and the covariance matrix of measurement noise, $\boldsymbol{R}$. The covariance matrices $\boldsymbol{Q}$ and $\boldsymbol{R}$ are defined as follows.

$$\boldsymbol{Q} = E\left[ww^T\right] \cdots\cdots (3)$$

$$\boldsymbol{R} = E\left[vv^T\right] \cdots\cdots (4)$$

where $\boldsymbol{Q}$ and $\boldsymbol{R}$ are nonnegative definite matrices and $E[\ ]$ denotes the expected value. For a steady-state Kalman filter in which the noise characteristics are constant, $\boldsymbol{Q}$ and $\boldsymbol{R}$ can be determined by using the testing simulations of the measurable signal, which is based on actual experimental data. The susceptibility of the Kalman filter to noise depends on the process noise covariance matrix $\boldsymbol{Q}$ and the measurement noise covariance matrix $\boldsymbol{R}$.

Figure 1 shows the algorithm of the Kalman filter. The Kalman filter uses a form of feedback control to estimate the state x. The filter predicts the state for a given time step and then obtains the feedback in the form of measurements for

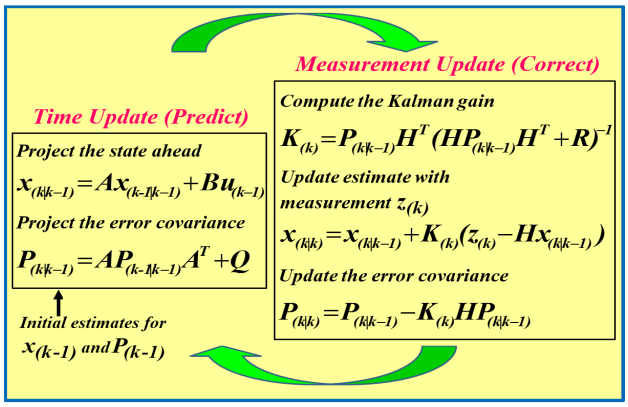

Fig. 1. Recursive adaptive Kalman filter algorithm

the corresponding time step, corrupted by noise. The current state and the estimation error are projected forward in time by the predictor equations as described in (5) and (6).

$$x_{(k|k-1)} = \boldsymbol{A}x_{(k-1|k-1)} + \boldsymbol{B}u_{(k-1)} \cdots\cdots (5)$$

$$\boldsymbol{P}_{(k|k-1)} = \boldsymbol{A}\boldsymbol{P}_{(k-1|k-1)}\boldsymbol{A}^T + \boldsymbol{Q} \cdots\cdots (6)$$

where $\boldsymbol{P}$ is the estimate error covariance matrix derived from the variance between the predicted state estimation and the improved state estimation. The Kalman filter gain matrix $\boldsymbol{K}$, which is based on the total uncertainty measurement, is computed to minimize the error covariance using the following equation.

$$\boldsymbol{K}_{(k)} = \boldsymbol{P}_{(k|k-1)}\boldsymbol{H}^T(\boldsymbol{H}\boldsymbol{P}_{(k|k-1)}\boldsymbol{H}^T + \boldsymbol{R})^{-1} \cdots\cdots (7)$$

The next step is to update the prior state estimation and the prior error covariance. The actual measurement $z_{(k)}$ at every sampling time is incorporated into the previous estimations to obtain improved estimates using the corrector equations as follows.

$$x_{(k|k)} = x_{(k|k-1)} + \boldsymbol{K}_{(k)}(z_{(k)} - \boldsymbol{H}\boldsymbol{x}_{(k|k-1)}) \cdots\cdots (8)$$

$$\boldsymbol{P}_{(k|k)} = \boldsymbol{P}_{(k|k-1)} - \boldsymbol{K}_{(k)}\boldsymbol{H}\boldsymbol{P}_{(k|k-1)} \cdots\cdots (9)$$

3. Force-sensor-less Observer Approaches

This section presents the approaches for the synthesis of the force-sensor-less observer proposed in our previous works. These observers are designed for disturbance force estimation or load force estimation, and have been integrated with the Kalman filter in various motion control schemes.

3.1 Disturbance Observer for Force Estimation

A disturbance observer [6]–[8] is a technique for the estimation and compensation of the disturbance force without using a force sensor. A robust acceleration control is realized by using the DOB. The DOB estimates the parameter variation, nonlinear friction, and other disturbances into consideration as one state variable.

Figure 2 shows the block diagram of the conventional DOB with a motor model. Here, J_m denotes the motor inertia, K_t denotes the torque coefficient and the subscript n represents the nominal value. I_m is the motor torque current, θ_m is the angle and ω_m represents the motor speed. T_m denotes the motor torque and T_{dis} is the disturbance torque. The expression for the disturbance torque in Fig. 2 is described in many papers [28][29].

The dynamic equation of the motor is expressed by (10).

$$J_m\dot{\omega}_m = T_m - T_{dis} \cdots\cdots (10)$$

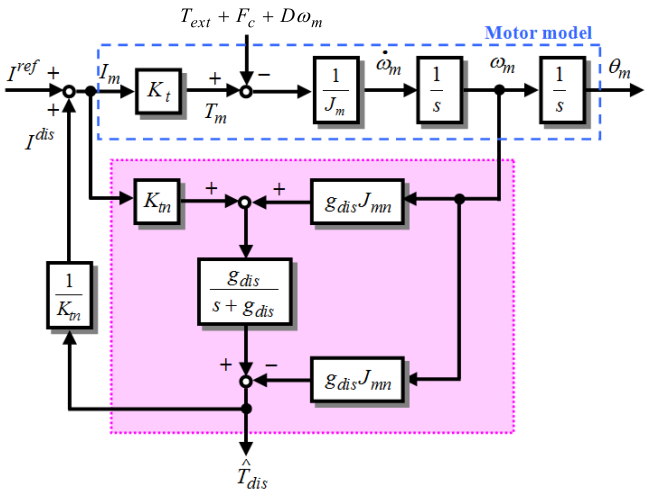

Fig. 2. Block diagram of the conventional disturbance observer

The total generated motor torque is given by (11).

$$T_m = K_t I_m \cdots\cdots (11)$$

The disturbance torque T_{dis} is defined as the total load torque applied on the motor including the effect of parameter variation and is represented as given in (12).

$$T_{dis} = T_{ext} + F_c + D\omega_m + (J_m - J_{mn})\dot{\omega}_m + (K_{tn} - K_t)I_m \cdots\cdots (12)$$

where T_{ext} denotes the reaction torque, F_c denotes the Coulomb friction and $D\omega_m$ denotes the viscous friction. $(J_m - J_{mn})\dot{\omega}_m$ is the torque due to the variation in self-inertia and $(K_{tn} - K_t)I_m$ is the torque ripple caused by the variation of the torque coefficient.

For the case where the motor parameter variations are zero, the disturbance force is given by (13).

$$T_{dis} = T_{ext} + F_c + D\omega_m \cdots\cdots (13)$$

From (10) and (11), the disturbance torque is expressed by (14).

$$\hat{T}_{dis} = K_{tn} I_m - J_{mn}\dot{\omega}_m \cdots\cdots (14)$$

Originally, equation (14) indicates that the disturbance torque is estimated based on the motor acceleration. The acceleration is estimated based on the position using the second derivative calculation. However, the second derivative of the position exhibits high noise level; therefore, a low-pass filter is used to filter out the high-frequency noise, and the DOB is derived with a low-pass filter. The DOB in Fig. 2 is derived with a first order low-pass filter, and the velocity information is usually obtained from the derivative of the position signal and a low-pass filter.

The estimated disturbance torque $\hat{T}_{dis}$ is obtained from the motor speed ω_m, and the motor current I_m, as given in (15).

$$\hat{T}_{dis} = \frac{g_{dis}}{s + g_{dis}}(K_{tn} I_m + g_{dis} J_{mn}\omega_m) - g_{dis} J_{mn}\omega_m \cdots\cdots (15)$$

where g_{dis} is the cut-off frequency of the low-pass filter used in the DOB to attenuate the high-frequency noise. g_{dis} determines the bandwidth of force sensing by the DOB.

The compensation current is computed from the estimated disturbance torque as follows.

$$I^{dis} = \frac{1}{K_{tn}}\hat{T}_{dis} \cdots\cdots (16)$$

By feeding back the compensation current, robust acceleration control is achieved.

3.2 Friction-free High-order Disturbance Observer for Force Estimation [15]

The performance of a force control system is determined by the accuracy of estimating the force. However, in practical applications, force estimation by the conventional DOB is deteriorated by friction phenomena. This also degrades the performance of the control system.

The elimination of friction improves force sensing and control performance. Our friction compensation method is the dithering technique, which is preferred to other techniques owing to its simple implementation. The effect of a dither signal is to smoothen the discontinuity due to friction. Therefore, by using the dithering method, we do not consider the friction model in our approach.

However, a dither signal introduces oscillatory disturbance in force estimation by the conventional DOB. Therefore, a force-sensing method capable of eliminating the effect of the oscillatory component in the force information is required. Based on this reasoning, we have proposed a high-order disturbance observer (HDOB) [15] to perform the force sensing function while reducing friction and the oscillatory component in the force information.

The dynamics of the oscillatory signal is modeled by a second-order system. The plant system of the HDOB is shown in Fig. 3. Therefore, the oscillatory torque is expressed as follows.

$$T'_{dis} = \frac{\omega_0^2}{s^2 + 2\zeta\omega_0 s + \omega_0^2} T_{dis} \cdots\cdots (17)$$

where ω_0 is the predetermined angular frequency of the additional periodic signal and ζ denotes the damping ratio. Here, T_{dis} is the torque signal without the oscillatory component, which is the step function expressed by (18); T'_{dis} is the oscillatory torque generated by superimposing the periodic signal on T_{dis}.

$$\frac{d}{dt}T_{dis} = 0 \cdots\cdots (18)$$

The model of the HDOB is realized based on the state space model in (19) and (20).

$$\dot{x} = \boldsymbol{A}x + \boldsymbol{B}u \cdots\cdots (19)$$

$$y = \boldsymbol{C}x \cdots\cdots (20)$$

where

$$x = \begin{bmatrix} \omega_m \\ \ddot{T}'_{dis} \\ \dot{T}'_{dis} \\ T'_{dis} \end{bmatrix}, \quad u = I_m, \quad y = \omega_m \cdots\cdots (21)$$

$$\boldsymbol{A} = \begin{bmatrix} 0 & 0 & 0 & -1/J_{mn} \\ 0 & -2\zeta\omega_0 & -\omega_0^2 & 0 \\ 0 & 1 & 0 & 0 \\ 0 & 0 & 1 & 0 \end{bmatrix}, \quad \boldsymbol{B} = \begin{bmatrix} K_{tn}/J_{mn} \\ 0 \\ 0 \\ 0 \end{bmatrix},$$

$$\boldsymbol{C} = \begin{bmatrix} 1 & 0 & 0 & 0 \end{bmatrix} \cdots\cdots (22)$$

Since the state variable ω_m is measurable, from the state matrices $\boldsymbol{A}$ and $\boldsymbol{B}$, the HDOB is defined using the minimum-order observer principles and the Ackermann method [30]. The state equations of the HDOB are obtained as described in (23) and (24).

$$\frac{d}{dt}\begin{bmatrix} \eta_1 \\ \eta_2 \\ \eta_3 \end{bmatrix} = \begin{bmatrix} a_0 & a_1 & a_2 \\ 1 & 0 & a_3 \\ 0 & 1 & a_4 \end{bmatrix}\begin{bmatrix} \eta_1 \\ \eta_2 \\ \eta_3 \end{bmatrix} + \begin{bmatrix} b_1 \\ b_2 \\ b_3 \end{bmatrix}\omega_m + \begin{bmatrix} c_1 \\ c_2 \\ c_3 \end{bmatrix} I_m \cdots\cdots (23)$$

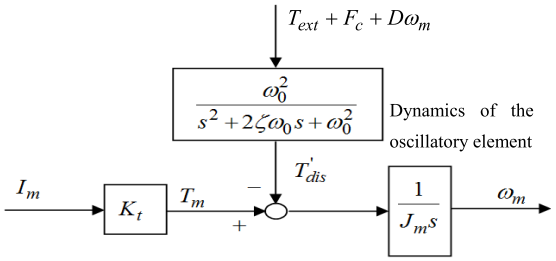

Fig. 3. Plant system of the high-order disturbance observer

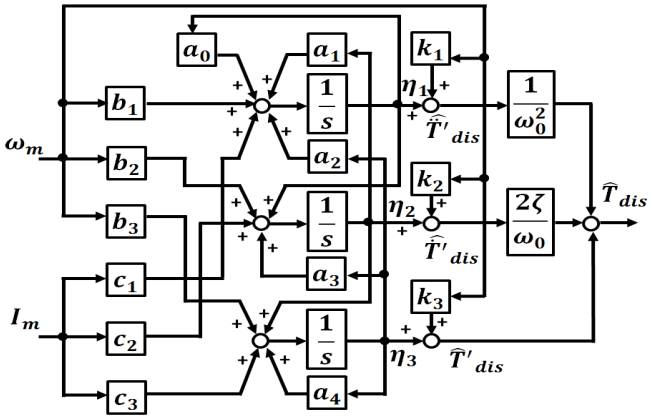

Fig. 4. Structure of the high-order disturbance observer

$$\begin{bmatrix} \ddot{T}'_{dis} \\ \dot{T}'_{dis} \\ T'_{dis} \end{bmatrix} = \begin{bmatrix} \eta_1 \\ \eta_2 \\ \eta_3 \end{bmatrix} + \begin{bmatrix} k_1 \\ k_2 \\ k_3 \end{bmatrix} \omega_m \cdots\cdots (24)$$

where

$$a_0 = -2\zeta\omega_0,\ a_1 = -\omega_0^2,\ a_2 = \frac{k_1}{J_{mn}},\ a_3 = \frac{k_2}{J_{mn}},\ a_4 = \frac{k_3}{J_{mn}} \cdots\cdots (25)$$

$$b_1 = -2\zeta\omega_0 k_1 - \omega_0^2 k_2 + \frac{k_1 k_3}{J_{mn}} \cdots\cdots (26)$$

$$b_2 = k_1 + \frac{k_2 k_3}{J_{mn}} \cdots\cdots (27)$$

$$b_3 = k_2 + \frac{k_3^2}{J_{mn}} \cdots\cdots (28)$$

$$c_1 = -\frac{K_{tn} k_1}{J_{mn}},\ c_2 = -\frac{K_{tn} k_2}{J_{mn}},\ c_3 = -\frac{K_{tn} k_3}{J_{mn}} \cdots\cdots (29)$$

where k_1, k_2 and k_3 are the elements of the observer gain matrix K_e which is derived by the Ackermann formula and is determined by the observer pole. The disturbance torque estimated by the HDOB is obtained using the estimated values $\hat{\dot{T}}'_{dis}$, $\hat{\dot{T}}'_{dis}$ and $\hat{T}'_{dis}$ as given in (30). The structure of the HDOB is illustrated in Fig. 4.

$$\hat{T}_{dis} = \frac{\hat{\dot{T}}'_{dis} + 2\zeta\omega_0 \hat{\dot{T}}'_{dis} + \omega_0^2 \hat{T}'_{dis}}{\omega_0^2} \cdots\cdots (30)$$

3.3 Instantaneous State Observer for Load Torque Estimation [21][22] In recent years, there has been a growing interest in robot motion control. Rapid and precise robot motion control is vital to improve productivity and quality. Robustness plays a central role in the design of a robot control scheme to achieve the above objective. Although the DOB is a common technique used for dynamic torque estimation and compensation to achieve robustness in robot systems, the high robustness of the robot manipulator is difficult to realize since the DOB exhibits estimation delay due to pole allocation. Therefore, we have proposed a load torque estimation method using the instantaneous state observer (ISOB) for industrial robots. The ISOB overcomes the estimation delay presented by the DOB, and attains instantaneous load torque estimation of a robot arm [21][22]. The load torque compensation based on the instantaneous load torque estimation makes the robot manipulator highly robust.

The ISOB is designed for the robot manipulator modeled as a two-inertia system with an integration of the accelerometer to measure the load-side acceleration. The state equation of the two-inertia system including the load torque τ_L is expressed as follows.

$$\frac{d}{dt}\begin{bmatrix} \omega_M \\ \omega_L \\ \theta_S \end{bmatrix} = \begin{bmatrix} -D_{Mn}/J_{Mn} & 0 & -K_{Sn}/R_{gn}J_{Mn} \\ 0 & -D_{Ln}/J_{Ln} & K_{Sn}/J_{Ln} \\ 1/R_{gn} & -1 & 0 \end{bmatrix} \begin{bmatrix} \omega_M \\ \omega_L \\ \theta_S \end{bmatrix} + \begin{bmatrix} K_{Tn}/J_{Mn} \\ 0 \\ 0 \end{bmatrix} I_{cmd} - \begin{bmatrix} 0 \\ 1/J_{Ln} \\ 0 \end{bmatrix} \tau_L \cdots\cdots (31)$$

where ω_M is motor velocity, ω_L is load-side velocity, and θ_S is torsional angle. J_M and J_L denotes motor side and load side inertia, respectively. D_M and D_L denotes motor side and load side viscosity coefficients, respectively. K_S is torsion spring constant, and R_g is gear ratio. I_{cmd} is the current command. Subscript n denotes the nominal value.

From (31), the derivative of the load-side velocity can be obtained directly using $\dot{\omega}_L = a_L$, when the load-side acceleration is detected using an acceleration sensor. Using a_L, the load torque τ_L is estimated as expressed in the following equation.

$$a_L = \dot{\omega}_L = -\frac{D_{Ln}}{J_{Ln}}\omega_L + \frac{K_{Sn}}{J_{Ln}}\theta_S - \frac{1}{J_{Ln}}\tau_L$$
$$\Leftrightarrow \tau_L = K_{Sn}\theta_S - D_{Ln}\omega_L - J_{Ln}a_L \cdots\cdots (32)$$

Equation (32) shows that the load torque τ_L is obtained instantaneously using the load-side acceleration a_L. To compensate for the initial state error, the state observer is designed using the observable output ω_M. The observer gain $k = \begin{bmatrix} k_1 & k_2 & k_3 \end{bmatrix}^T$ is designed to express the state observer of the two-inertia system. The state equation of the ISOB is presented as follows.

$$\frac{d}{dt}\begin{bmatrix} \hat{\omega}_M \\ \hat{\omega}_L \\ \hat{\theta}_S \end{bmatrix} = \begin{bmatrix} -\frac{D_{Mn}}{J_{Mn}} - k_1 & 0 & -\frac{K_{Sn}}{R_{gn}J_{Mn}} \\ -k_2 & 0 & 0 \\ \frac{1}{R_{gn}} - k_3 & -1 & 0 \end{bmatrix} \begin{bmatrix} \hat{\omega}_M \\ \hat{\omega}_L \\ \hat{\theta}_S \end{bmatrix} + \begin{bmatrix} \frac{K_{Tn}}{J_{Mn}} \\ 0 \\ 0 \end{bmatrix} I_{cmd} + \begin{bmatrix} 0 \\ 1 \\ 0 \end{bmatrix} a_L + \begin{bmatrix} k_1 \\ k_2 \\ k_3 \end{bmatrix} \omega_M \cdots\cdots (33)$$

$$\hat{\tau}_L = \begin{bmatrix} 0 & -D_{Ln} & K_{Sn} \end{bmatrix} \begin{bmatrix} \hat{\omega}_M \\ \hat{\omega}_L \\ \hat{\theta}_S \end{bmatrix} - J_{Ln}a_L \cdots\cdots (34)$$

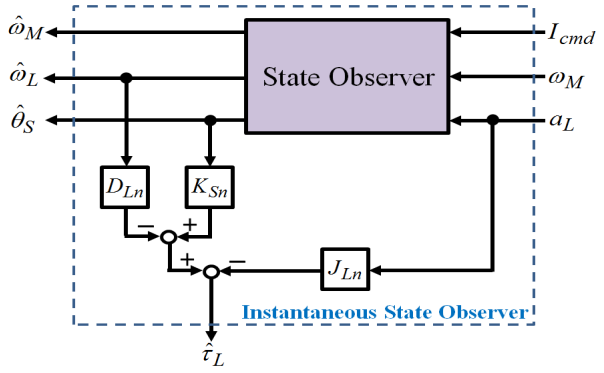

Fig. 5. Block diagram of the instantaneous state observer

Equations (33) and (34) show that the ISOB consists of a state observer for a two-inertia system with an acceleration input, and achieves instantaneous load torque estimation using the estimated state variables $\hat{\omega}_L$, $\hat{\theta}_S$, and the measured load-side acceleration a_L. The block diagram of the ISOB is shown in Fig. 5.

In our research, the acceleration sensor, which is used with the ISOB, is a DC-response accelerometer (PCB Piezotronics: 3711B) with bandwidth of 1 kHz. The load torque estimation delay by the ISOB is not dependent on the observer pole. However, the estimation delay is determined by the bandwidth of acceleration sensor.

Moreover, the accelerometer has offset and high-frequency noises. For eliminating the sensor offset: because we use an acceleration sensor capable of measuring DC response, the sensor can detect gravitational acceleration. Therefore, we calibrate the offset caused by acceleration of gravity in the measured acceleration easily. For suppressing high-frequency noises: because the bandwidth of acceleration sensor is 1 kHz, the noise with frequency higher than 1 kHz is suppressed. To suppress the noise with frequency smaller than 1 kHz in acceleration signal, we apply the VNC Kalman filter to estimate the load acceleration. The VNC Kalman filter reduces the vibration of impulsive responses and suppress the high-frequency noises in acceleration signal. Figure 22 in Section 4.3 shows the effect of noise suppression using VNC Kalman filter.

4. Applications of Motion Control based on Kalman Filter and Disturbance Observer

This section introduces the methods to integrate the Kalman filter and the DOB in specific applications of motion control and provides evaluations on the performance of the control schemes.

4.1 Motion Control Using Position-sensor-based Kalman Filter and Disturbance Observer [14]–[16]

4.1.1 Position-sensor-based Kalman Filter for Velocity Estimation The disturbance observers described in Sections 3.1 and 3.2 use the information of the current reference and motor velocity as inputs to estimate the disturbance force. Hence, the performance of force estimation by the DOB is related to how the velocity is accurately estimated. Conventionally, the motor velocity is estimated based on the derivative of the position signal with respect to time. The position information is simply obtained from an encoder.

However, the conventional velocity estimation method is susceptible to the effect of derivative noise. Hence, the force-sensing performance of the DOB is degraded by noise. Noise also limits the bandwidth of force sensing by the DOB. Therefore, to address the noise problem, the Kalman filter is utilized for velocity estimation. Using the Kalman filter, we can reduce the noise of the measurement system effectively. As a result, the performance of the control system and the force-sensing bandwidth is improved.

Here, velocity estimation by the Kalman filtering is based on the position information measured by an encoder. The state, control input and observation matrices corresponding to (1) and (2) are described in (35).

$$\boldsymbol{A} = \begin{bmatrix} 1 & T_s & 0.5T_s^2 \\ 0 & 1 & T_s \\ 0 & 0 & 1 \end{bmatrix}, \ \boldsymbol{B} = \begin{bmatrix} 0 \\ 0 \\ 0 \end{bmatrix}, \ \boldsymbol{H} = \begin{bmatrix} 1 & 0 & 0 \end{bmatrix} \cdots\cdots (35)$$

$x_{(k)}$ is the vector of the estimated state, including the position, velocity, and acceleration; $z_{(k)}$ is the measured position, which is corrupted by noise. T_s is the sampling time of control system. The estimation process by the Kalman filter is then carried out as given in (5)–(9) in Section 2.

4.1.2 Force Control of a Linear Shaft Motor System Using Position-sensor-based Kalman Filter (PKF) and Disturbance Observer [14] Figure 6 shows the block diagram of the force control using position-sensor-based Kalman filter and disturbance observer. Here, the velocity estimation is performed by PKF using only the encoder output. The DOB estimates the disturbance force using motor current reference and velocity estimated by PKF. This method is applied for a linear shaft motor. The control algorithm is implemented in FPGA to shorten the sampling time so that the force sensing bandwidth of DOB can be widened by increasing the cut-off frequency of the low-pass filter used in the DOB. Figure 7 shows experimental devices of force control system.

The effectiveness of this method is evaluated through experiments of force control using DOB with conventional velocity estimation and force control using DOB with PKF. In the experiments, the force sensing bandwidth of DOB is set to 6280 rad/s, the cut-off frequency of conventional velocity estimation is also set to 6280 rad/s, and the force command is a constant of 0.5 N. The motor movements are stimulated by human force applied on the motor. The impact motions are caused by the collision between the motor and a rubber piece. Figure 8 shows the experimental results of force responses. The force response estimated by the DOB with conventional velocity estimation is totally corrupted by noise at the bandwidth of 6280 rad/s as shown in Fig. 8(a). Whereas in Fig. 8(b), the DOB using PKF attains the smooth force responses with very low noise level. These results indicate that the DOB using PKF provides the improved force sensing performance in terms of noise reduction and widening force sensing bandwidth.

4.1.3 Force Control of a Ball-screw System Using Friction-free High-order Disturbance Observer and Position-sensor-based Kalman Filter [15] Figure 9 shows the force control of a ball-screw system using friction-free HDOB and PKF. Here, the velocity estimation is also performed by PKF using the encoder output only. The HDOB uses motor current reference and velocity estimated by PKF

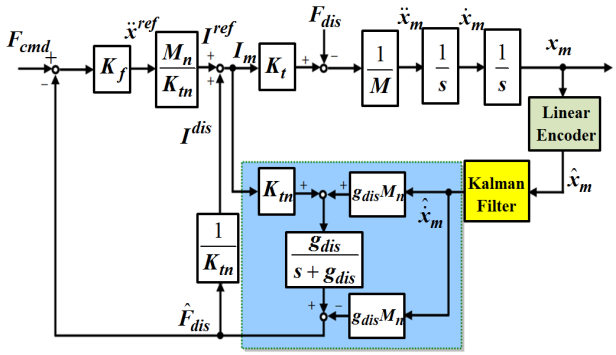

Fig. 6. Block diagram of force control using PKF and DOB

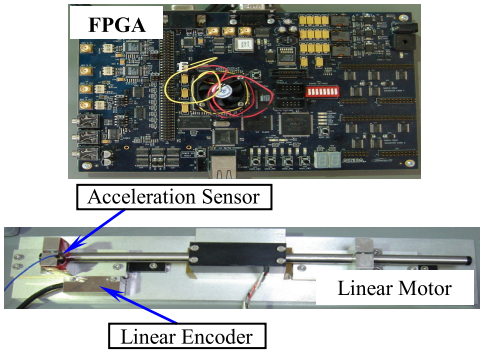

Fig. 7. Experimental devices for force control of a linear shaft motor

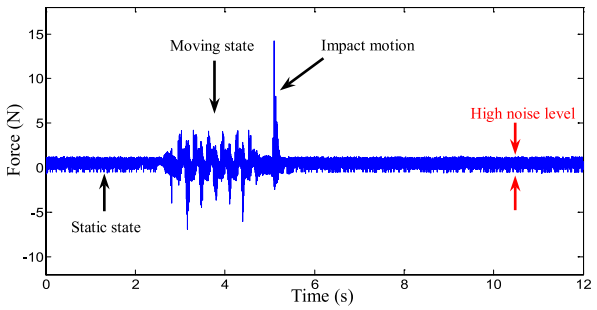

(a) Estimated by DOB using conventional velocity estimation

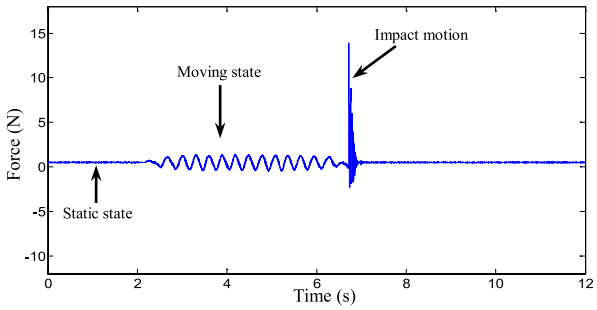

(b) Estimated by DOB using PKF

Fig. 8. Force responses at force sensing bandwidth of 6280 rad/s

to estimate the disturbance force with the elimination of oscillatory component caused by dither. This method is applied for a ball-screw system exhibiting high friction. The friction compensation is based on dithering method with dither frequency of 5 Hz. The control algorithm is also implemented in FPGA to shorten the sampling time and make it possible to widen the force sensing bandwidth of HDOB by increasing observer pole.

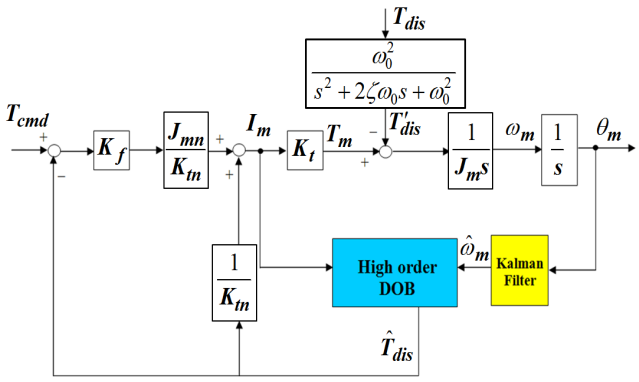

(a) Block diagram of the force control system

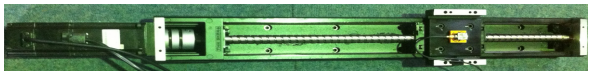

(b) Experimental device: Servo motor with a ball-screw

Fig. 9. Force control based on HDOB and PKF

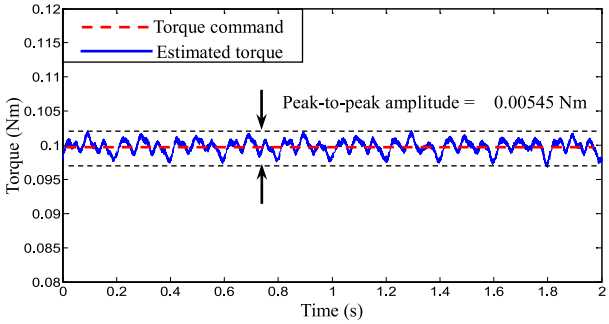

Fig. 10. Torque response estimated by conventional DOB distorted by friction

The design of dither signal is as follows [15]. In our paper, we selected $\zeta = 0$ so that the dither signal is an undamped oscillation, because we desire that the dither signal always has effect during control system operation. The amplitude of dither signal is determined experimentally so that it does not cause vibration in the control system, and is based on the peak-to-peak amplitude of torque signal deteriorated by friction (ΔT). Here, the peak-to-peak amplitude of torque signal is 0.00545 Nm as shown in Fig. 10. Hence, the corresponding current value is $\Delta I = \Delta T / K_{tn} = 0.011$ A, with $K_{tn} = 0.498$ Nm/A. The amplitude of dither signal is selected with a value higher than ΔI so that the effect of friction can be reduced provided that it does not generate system vibration. In this paper, the dither is added to the current reference and has the amplitude of 0.015 A.

For determination of dither frequency, we conducted the experiments of force control using HDOB with different frequencies of dither signal, under conditions of constant torque command of 0.1 Nm and constant velocity of 10.5 rad/s. Here, the HDOB with dither signal performs the force estimation with the observer pole of 300 rad/s. We investigate the relationship between the dither frequency and the peak-to-peak amplitude of torque signal estimated by HDOB. The experimental results are shown in Fig. 11. The results show that the peak-to-peak amplitude of torque signal significantly decreases at dither frequency of 5 Hz, then continues to a little decrease and reaches the saturation state at dither frequencies 10 Hz, 15 Hz, and 20 Hz. These results indicate that

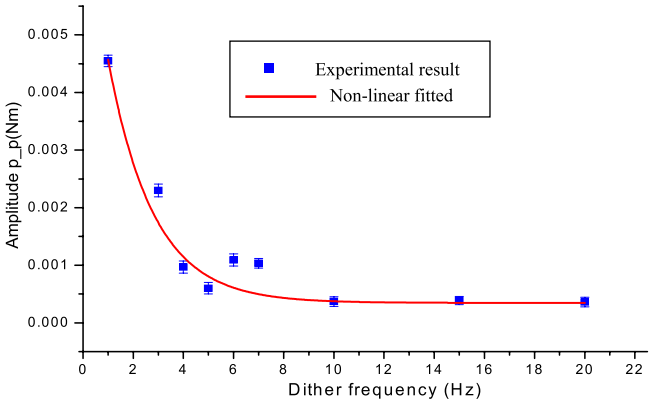

Fig. 11. Experimental results of relationship between dither frequency and peak-to-peak amplitude of torque estimated by HDOB

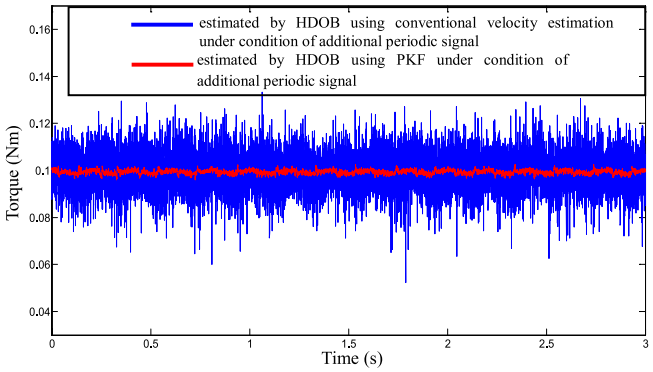

Fig. 12. Torque responses estimated by HDOB using Kalman filter and HDOB using conventional velocity estimation with observer pole at 1000 rad/s

friction in force estimation is effectively reduced by selecting dither signal with frequency of 5 Hz or of higher value. Therefore, we determine to use the 5 Hz-dither signal with HDOB for the force control of ball-screw system.

To verify the effectiveness of this method, the force control experiment of a ball-screw system was carried out to perform the torque tracking with a constant torque command of 0.1 Nm. The observer pole is set to 1000 rad/s. Figure 12 presents torque responses estimated by HDOB using conventional velocity estimation and HDOB using PKF (both with additional dither signal). The signal estimated by the HDOB without Kalman filter is highly corrupted by very high noise level when observer pole is set to 1000 rad/s. However, the signal estimated by the HDOB using PKF is significantly improved because the noise in the estimated torque is suppressed effectively and the oscillatory disturbance caused by dither is eliminated. The results confirm that the force control using the HDOB and the Kalman filter with a dither signal achieves high-performance force sensing with a widened bandwidth of 1000 rad/s based on friction-free and noise-free force observation.

Moreover, Fig. 13 presents the comparison of the torque estimations between the conventional DOB using Kalman filter (without dither signal) and the HDOB using Kalman filter (with dither signal) at force sensing bandwidth of 1000 rad/s. The estimated torque without dither has unsmooth response caused by friction. For the HDOB with the Kalman filter and

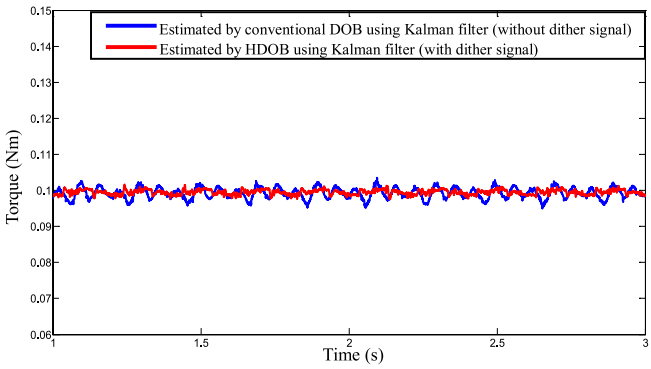

Fig. 13. Torque responses estimated by conventional DOB using Kalman filter (without dither signal) and HDOB using Kalman filter (with dither signal) at force sensing bandwidth of 1000 rad/s

with the dither signal, the effect of friction in the estimated torque is reduced, and the oscillatory component caused by dither is also eliminated. These results confirm the effectiveness of dither signal inputting.

4.2 Motion Control Using Multi-sensor-based Kalman Filter and Disturbance Observer [14] [17]–[20]

4.2.1 Multi-sensor-based Kalman Filter (MKF) for Velocity Estimation Although the position-sensor-based Kalman filter can reduce noise efficiently and the DOB can obtain improved force estimation, the limitation of this method is that the accuracy and bandwidth of the measuring system are subject to the performance of the encoder. For the condition of only position measurement, imprecise velocity estimation often occurs during impact motions with high accelerations due to bandwidth limitation of the measurement device. Therefore, a multi-sensor fusion in Kalman filter is employed to obtain the accurate velocity estimation, especially in impulsive responses.

In our system, we use the linear encoder Renishaw RGH24Y with the maximum speed of 0.25 m/s and resolution of 0.1 μm. The control sampling time is 5 μs, and we obtain position information in every control sampling period. Hence, the bandwidth of the position measurement is 100 kHz. The performance of velocity estimations by PKF and MKF are dependent on the measurement devices and the bandwidth of Kalman filter, which is dependent on the noise characteristics ($\boldsymbol{R}$ and $\boldsymbol{Q}$ matrices). Figures 14 and 15 show the simulation results of the bandwidth limitation of estimations using PKF and MKF.

As shown in Fig. 14, the PKF has the position-estimation bandwidth of 1130 rad/s. Since the PKF uses only position sensor as the input to estimate velocity, the bandwidth of position estimation determines the bandwidth of velocity estimation by the PKF. However, for the MKF, the position-estimation bandwidth is 940 rad/s while the acceleration estimation has a wider bandwidth of 7800 rad/s as shown in Fig. 15. Since the MKF uses both position sensor and acceleration sensor as the inputs to estimate velocity, these bandwidths determine the bandwidth of velocity estimation by the MKF. The wider bandwidth of acceleration estimation contributes to the velocity estimation in impact motion with high frequency accelerations. Therefore, the velocity estimation in impact motions by the MKF is more accurate than the PKF

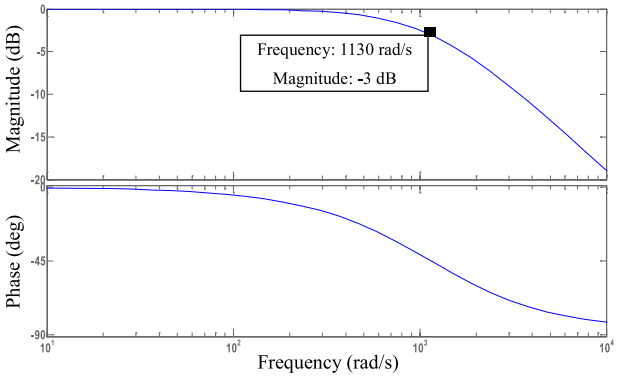

Fig. 14. Bandwidth of position estimation by PKF

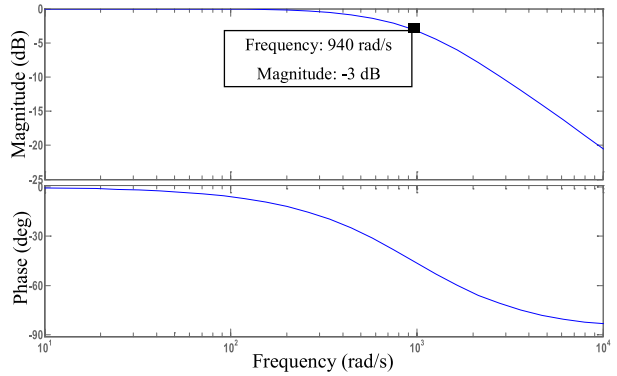

(a) Bandwidth of position estimation

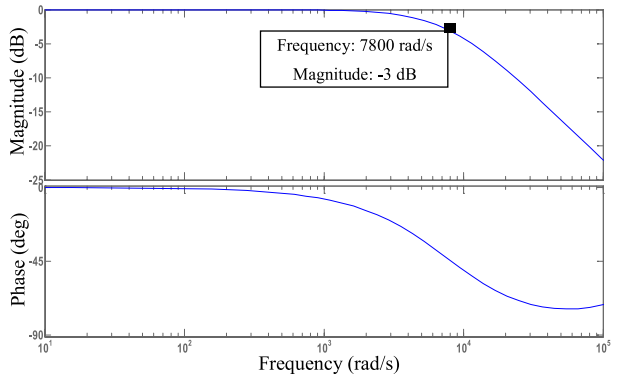

(b) Bandwidth of acceleration estimation

Fig. 15. Bandwidth of estimations by MKF

because the velocity estimation performance by the PKF is limit by position estimation bandwidth. With the improved velocity estimation by MKF, it is possible for the DOB to achieve high force sensing performance.

In the multi-sensor measuring system, the measurement process model is also given by (1) and (2). $x_{(k)}$ is still the state vector of position, velocity and acceleration. $z_{(k)}$ is the vector of measured variables comprising the position measured by encoder and the acceleration measured by accelerometer. Hence, the state, control input and observation matrices are described as follows.

$$\boldsymbol{A} = \begin{bmatrix} 1 & T_s & 0.5T_s^2 \\ 0 & 1 & T_s \\ 0 & 0 & 1 \end{bmatrix}, \quad \boldsymbol{B} = \begin{bmatrix} 0 \\ 0 \\ 0 \end{bmatrix}, \quad \boldsymbol{H} = \begin{bmatrix} 1 & 0 & 0 \\ 0 & 0 & 1 \end{bmatrix} \quad \cdots\cdots\cdots\cdots\cdots (36)$$

The estimation process by Kalman filter is then performed as described in (5)–(9) in Section 2. The design of the covariance matrices $\boldsymbol{Q}$ and $\boldsymbol{R}$ for MKF is described as follows.

$$\boldsymbol{Q} = E\left[ww^T\right] = \begin{bmatrix} Q_{11} & 0 & 0 \\ 0 & Q_{22} & 0 \\ 0 & 0 & Q_{33} \end{bmatrix} \cdots\cdots\cdots\cdots (37)$$

$$\boldsymbol{R} = E\left[vv^{\mathrm{T}}\right] = \begin{bmatrix} R_{11} & 0 \\ 0 & R_{22} \end{bmatrix} \cdots\cdots\cdots\cdots\cdots\cdots (38)$$

where $\boldsymbol{Q}$ and $\boldsymbol{R}$ are nonnegative definite matrices and $E[\ ]$ denotes the expected value. Elements of $\boldsymbol{Q}$ and $\boldsymbol{R}$ are defined as follows.

$$R_{11} = Var\left[\Delta x_m\right] \cdots\cdots\cdots\cdots\cdots\cdots\cdots\cdots (39)$$

$$R_{22} = Var\left[\Delta \ddot{x}_m\right] \cdots\cdots\cdots\cdots\cdots\cdots\cdots\cdots (40)$$

$$Q_{11} = Var\left[\Delta x_e\right] \cdots\cdots\cdots\cdots\cdots\cdots\cdots\cdots (41)$$

$$Q_{22} = Var\left[\Delta \dot{x}_e\right] \cdots\cdots\cdots\cdots\cdots\cdots\cdots\cdots (42)$$

$$Q_{33} = Var\left[\Delta \ddot{x}_e\right] \cdots\cdots\cdots\cdots\cdots\cdots\cdots\cdots (43)$$

where $Var\ [\ ]$ denotes variance, Δx_m is the difference between the measured position and the desired position, $\Delta \ddot{x}_m$ is the difference between the measured acceleration and the desired acceleration. Δx_e, $\Delta \dot{x}_e$, and $\Delta \ddot{x}_e$ are the differences between the predicted values of position, velocity, and acceleration, and the desired values of position, velocity and acceleration, respectively. Δx_m is calculated from the sets of position data measured by an encoder. $\Delta \ddot{x}_m$ is calculated from the sets of acceleration data measured by an acceleration sensor. Δx_e, $\Delta \dot{x}_e$ and $\Delta \ddot{x}_e$ are calculated from the sets of filter's predicted values of position, velocity, and acceleration, given the corresponding sets of sample data of position measured by encoder and data of acceleration measured by acceleration sensor. Variances of Δx_m, $\Delta \ddot{x}_m$, Δx_e, $\Delta \dot{x}_e$ and $\Delta \ddot{x}_e$ are computed as follows.

$$Var\left[X\right] = \frac{|X_1 - \mu|^2 + \ldots + |X_n - \mu|^2}{n} \cdots\cdots\cdots\cdots (44)$$

where

$$\mu = \frac{X_1 + X_2 + \ldots + X_n}{n} \cdots\cdots\cdots\cdots\cdots\cdots\cdots (45)$$

X stands for Δx_m, $\Delta \ddot{x}_m$, Δx_e, $\Delta \dot{x}_e$ or $\Delta \ddot{x}_e$, and n is the data number of the sample data set. The value of matrix $\boldsymbol{R}$ can be easily determined based on the available measured position data, and equations (39), (40), (44) and (45). The values of matrix $\boldsymbol{Q}$ are selected by trial and error. The trial and error process is carried out by fixing $\boldsymbol{R}$ value, running Kalman filter offline with the data set of measured position, obtaining the data sets of predicted values, calculating $\boldsymbol{Q}$ values based on (41), (42), (43), (44) and (45), and running filter again. The selected values of Q are those enabling the estimated state of filter to achieve the proper values.

Figure 16 shows the experimental results to evaluate the velocity estimation of the Kalman filter using multi-sensor and that of the Kalman filter using only encoder. The experimental system is shown in Fig. 7. These results show that there is good agreement between the velocity responses estimated by both methods except for the impact motion response. During the impact motion with high acceleration, the velocity response estimated by MKF is much improved as shown in Fig. 16(b). These results confirm the advantage of acceleration measurement in obtaining accurate velocity estimation by Kalman filter.

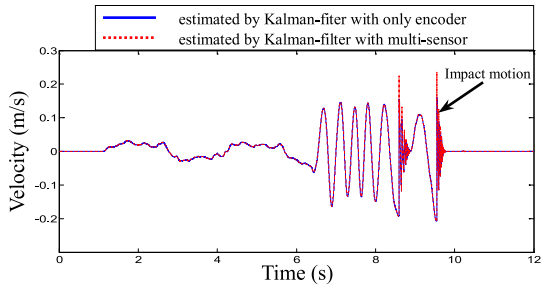

(a) Velocity responses

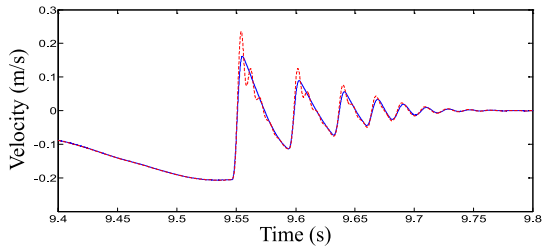

(b) Magnification of impact motion in (a)

Fig. 16. Experimental results of velocity estimation

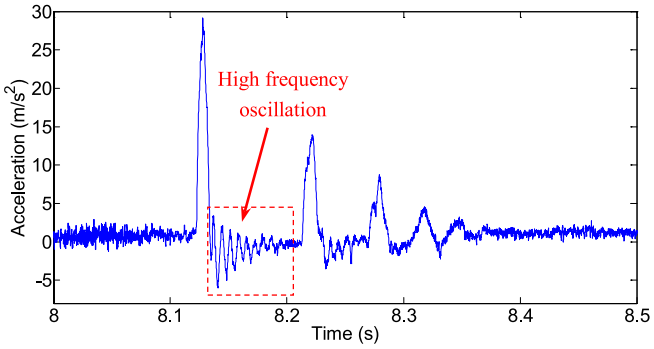

Fig. 17. Acceleration response of impact motion measured by acceleration sensor

To confirm the accuracy of the velocity estimation by MKF in Fig. 16, we investigate the impact acceleration response measured by acceleration sensor as shown in Fig. 17. The impact acceleration response has the high frequency oscillations that are reflected in the velocity estimation by the MKF in Fig. 16. In contrast, the velocity estimation by PKF has no such high frequency oscillations during impact motion. It is the acceleration information that contributes to the estimation of velocity during impact motion using the MKF.

4.2.2 Force Control of a Linear Shaft Motor System Using Multi-sensor-based Kalman Filter (MKF) and Disturbance Observer [14] Figure 18 shows the block diagram of the force control using multi-sensor-based Kalman filter and disturbance observer. Here, the velocity estimation is performed by MKF using multi-sensor information of encoder and acceleration sensor. The DOB estimates the disturbance force using motor current reference and velocity estimated by MKF.

This method is applied for a linear shaft motor. The control algorithm is implemented in FPGA to shorten the sampling time such that the force sensing bandwidth of DOB can be widened by increasing the cut-off frequency of the low-pass filter used in the DOB. The effectiveness of this approach is evaluated through experiments of force control using DOB

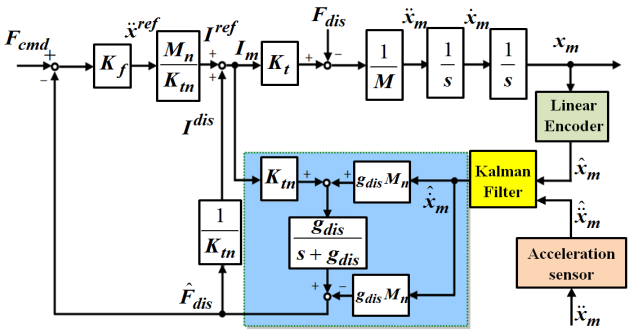

Fig. 18. Block diagram of force control using Multi-sensor-based Kalman filter and disturbance observer

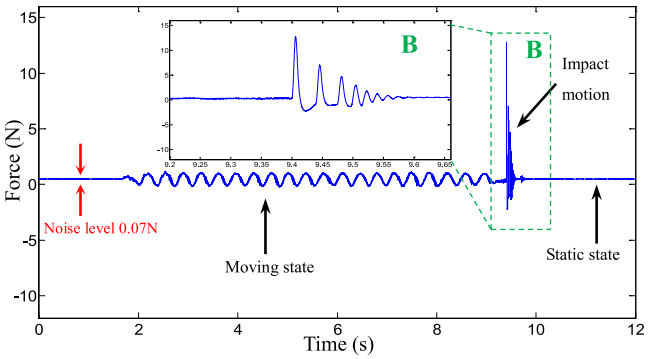

(a) Estimated by Position-sensor-based Kalman filter and DOB

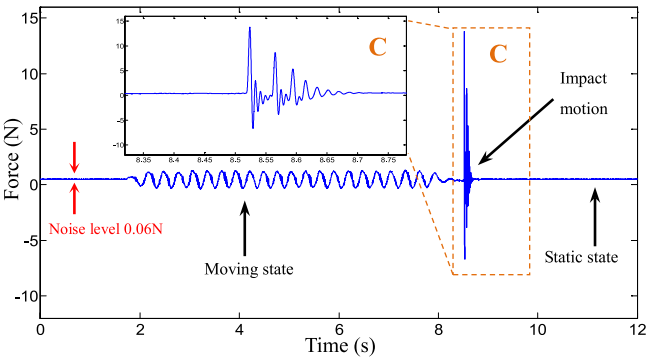

(b) Estimated by Multi-sensor-based Kalman filter and DOB

Fig. 19. Force responses at force sensing bandwidth of 6280 rad/s

with PKF and force control using DOB with MKF. In the experiments, the force sensing bandwidth of DOB is set to 6280 rad/s, the cut-off frequency of conventional velocity estimation is also set to 6280 rad/s, and the force command is a constant of 0.5 N. The motor movements are stimulated by human force applied to the motor. The impact motions are caused by collision between the motor and a rubber piece. Figure 19 displays the force responses at the force sensing bandwidth of 6280 rad/s. The results show that both the DOB using MKF and the DOB using PKF obtain the smooth force responses with very low peak-to-peak noise levels. From these results, it is clear that both methods provide the good force sensing performance. However, since the DOB with MKF achieves accurate velocity estimation during the impact motion by the Kalman filter with multi-sensor, the impact force response of this method is improved significantly compared to that of the DOB using Kalman filter with only encoder. These results confirm that the combination of multi-sensor-based Kalman filter and the DOB attains the high

performance force sensing based on the improved velocity information.

4.3 Motion Control of Industrial Robot Using Variable Noise-Covariance Kalman Filter Based Instantaneous State Observer [21)–(23)] As presented in Section 3.3, the load torque compensation based on instantaneous load torque estimation makes the robot manipulator highly robust. The ISOB is designed for a two-inertia system with the integration of an acceleration sensor to measure the load-side acceleration. The performance of load-side torque estimation using the ISOB is related to the measurement of load-side acceleration. Since the ISOB employs an acceleration sensor to directly obtain the load-side acceleration information, the measured acceleration signal is susceptible to the effect of noise. Hence, the torque estimation performance of the ISOB is also affected by the noise problem.

To address the noise problem, a Kalman filter is utilized for load-side acceleration estimation. Normally, the Kalman filter operates under the assumption that the noise characteristics of the measuring process remain constant at every time step. However, in practice, the noise characteristics are uncertain. Especially, in our research, the measurement noise characteristics the of load-side acceleration significantly change during impulsive acceleration responses. Therefore, to suppress the noise in acceleration signal effectively, we proposed an acceleration estimation based on a variable noise-covariance (VNC) Kalman filter. Consequently, the integration of the VNC Kalman filter with the ISOB enhances the performance of ISOB. The VNC Kalman filter estimates the state of the measuring process formulated in equations (1) and (2). Here, $x_{(k)}$ is the estimated load-side acceleration; $z_{(k)}$ is the measured acceleration information, which is corrupted by noise. The state, control input and observation matrices are now given as follows.

$$\boldsymbol{A} = 1, \quad \boldsymbol{B} = 0, \quad \boldsymbol{H} = 1 \cdots\cdots\cdots\cdots\cdots\cdots\cdots\cdots (46)$$

The covariance matrix of process noise, $\boldsymbol{Q}$, and the covariance matrix of measurement noise, $\boldsymbol{R}$, are defined as indicated in equations (3) and (4). For a steady-state Kalman filter in which the noise characteristics are constant, $\boldsymbol{Q}$ and $\boldsymbol{R}$ can be determined using the testing simulations of the measurement sensor signal, which is based on the actual experimental data.

In our research, the noise characteristics of the acceleration measurement are considered to be uncertain. Hence, a variable-noise-covariance estimation is executed to determine the value of $\boldsymbol{R}$ during the operation of Kalman filter. The estimation of noise covariance $\boldsymbol{R}$ is performed as follows.

$$\boldsymbol{R} = \sigma \quad \text{when} \quad (\sigma > \boldsymbol{R}_{St}) \cdots\cdots\cdots\cdots\cdots\cdots\cdots (47)$$

$$\boldsymbol{R} = \boldsymbol{R}_{St} \quad \text{when} \quad (0 < \sigma \leq \boldsymbol{R}_{St}) \cdots\cdots\cdots\cdots\cdots\cdots (48)$$

where

$$\sigma = \sqrt{\frac{1}{N}\sum_{i=1}^{N}(a_i - M)^2}, \quad M = \frac{1}{N}\sum_{i=1}^{N} a_i \cdots\cdots\cdots (49)$$

$\boldsymbol{R}_{St}$ is the measurement noise covariance corresponding to the steady-state Kalman filter. N is the length of the measured acceleration data set used to determine $\boldsymbol{R}$ at every sampling time. a_i is the i$^{\text{th}}$ element of the N-element-acceleration data set. During the filter operation, the acceleration data set is updated every sampling cycle. N is dependent on the sampling time of control system and is selected by testing simulations of actual acceleration signal such that the characteristics of high frequency and large variation of the noise at impulsive acceleration responses are captured by (49). The estimation of the variable noise covariance $\boldsymbol{R}$ is used to run the Kalman filter for load-side acceleration estimation. The estimation process by Kalman filter is then performed as described in (5)–(9) in Section 2. The updated acceleration estimation by the VNC Kalman filter is applied to the ISOB for load torque estimation. The block diagram of the VNC-Kalman-filter-based ISOB is shown in Fig. 20.

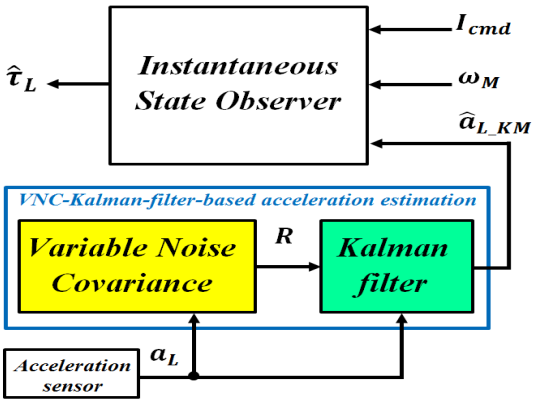

Fig. 20. Block diagram of the VNC-Kalman-filter-based ISOB

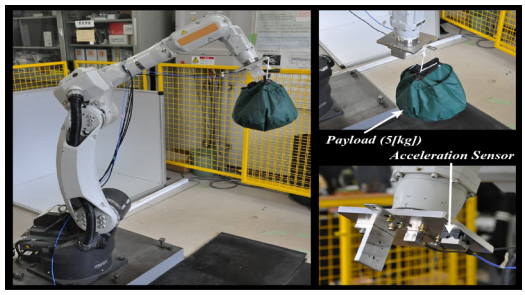

Fig. 21. Experimental system of industrial robot arm

In order to verify the effectiveness of the VNC-Kalman-filter-based ISOB, the numerical simulation results based on the speed-control experimental data of a robot arm are presented. The speed-control experiment was carried out using the upper arm of the industrial robot. Figure 21 shows the overall view of the experimental equipment. The robot arm was operated at the constant speed of 30 rad/s so that the end-effector payload fell at a downward posture. The falling of the end-effector payload resulted in the impulsive motion of the robot arm and the impulsive acceleration response. Experimental data sets of I_{cmd}, ω_M, and a_L were obtained during the speed-control operation. These experimental data sets are used to perform the numerical simulation of the VNC-Kalman-filter-based ISOB. The simulations were conducted with observer pole of 200 rad/s.

Figure 22 shows the accelerations estimated by the VNC-Kalman filter compared with the actual acceleration signal measured by the acceleration sensor. These results show that VNC-Kalman filter reduces noise in the acceleration estimation, and significantly reduces vibration in the impulsive response. During the impulsive response, the noise covariance

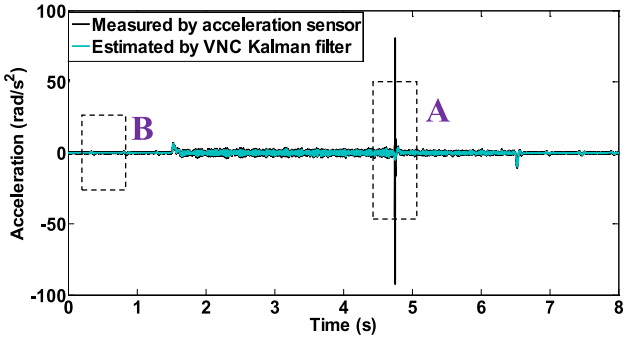

(a) Load-side acceleration

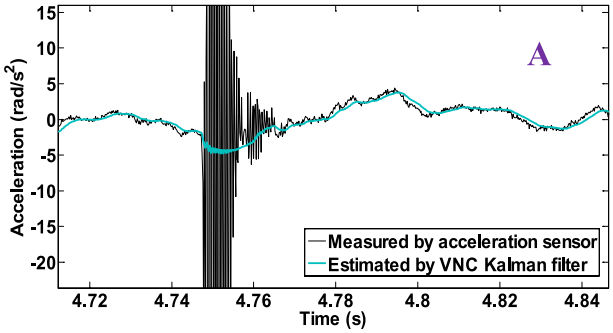

(b) Magnification of impulsive response (A area)

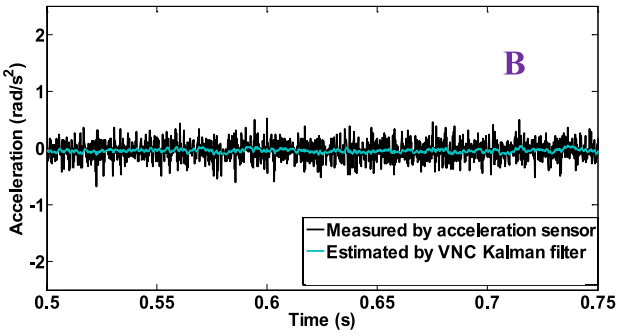

(c) Magnification of steady state (B area)

Fig. 22. Load-acceleration responses

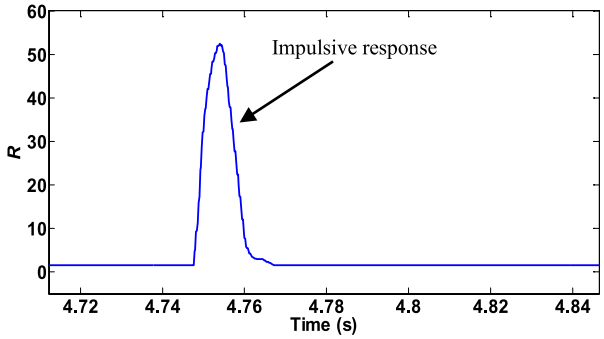

Fig. 23. Estimation of variable noise covariance $\boldsymbol{R}$

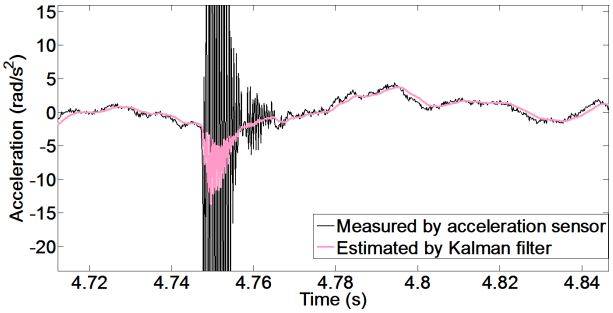

Fig. 24. Impulsive load-acceleration responses estimated by Kalman filter

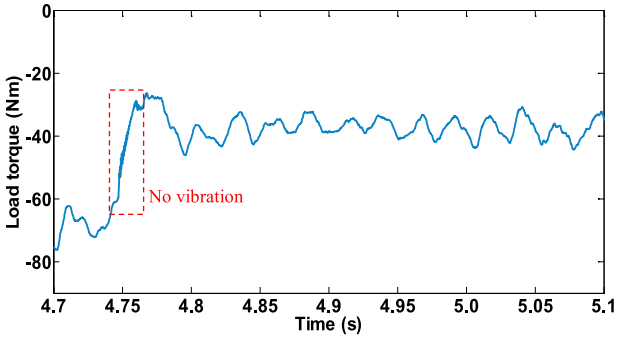

Fig. 25. Load torque estimated by VNC-Kalman-filter-based ISOB

$\boldsymbol{R}$ of the VNC Kalman filter changes and has high values as shown in Fig. 23. Because the bandwidth of estimation by Kalman filter is dependent on $\boldsymbol{R}$ and $\boldsymbol{Q}$, the changing of $\boldsymbol{R}$ make the estimation bandwidth change. Hence, the VNC Kalman filter reduces the vibration of impulsive response to small amplitude effectively, and still reflects the impulsive response in the acceleration estimation. However, the amplitude of impulsive response is reduced to a certain extent due to estimation bandwidth limitation during impulsive response. For the Kalman-filter-based acceleration estimation, the noise covariance $\boldsymbol{R}$ is constant during impulsive response. The results in Fig. 24 show that the Kalman-filter-based acceleration estimation cannot suppress the vibration effectively.

The load torque estimated by the VNC-Kalman-filter-based ISOB is presented in Fig. 25. This result proves that the estimated impulsive load torque has no effect of vibration due to superior acceleration estimation by the VNC-Kalman filter. The above results confirm that this method achieves high performance load torque estimation, and is feasible to realize the high-performance load acceleration control of industrial robots.

4.4 Force Control Using Kalman Filter Based Force Sensing with Periodic Component Extraction [24] In Section 3.2, we introduced the HDOB with dither signal for force sensing operation and elimination of periodic disturbance in force estimation. However, the design of the HDOB is motivated by a state-space approach and the force estimation is noisy when the observer pole is increased.

Besides, in Section 4.1.3, the force control of a ball-screw system uses the HDOB with velocity estimation based on the Kalman filter. Since motor speed is the input of the HDOB, using Kalman filter effectively reduces noise in velocity estimation, and reduces noise in force estimation by HDOB to a certain extent.

However, since the design of the HDOB itself does not consider the noise suppression of the estimations of T'_{dis}, $\dot{T}'_{dis}$ and $\ddot{T}'_{dis}$, the force estimation by the HDOB becomes noisy when the observer pole is increased. Therefore, even when the Kalman filter is employed for velocity estimation, this method has less potential to further widen the force sensing bandwidth.

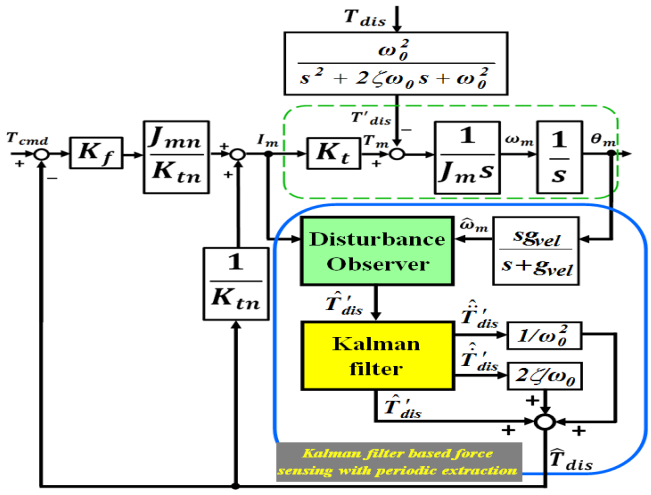

Fig. 26. Force control using Kalman-filter-based force sensing with periodic component extraction

To address the noise problem, the estimations of T'_{dis}, $\dot{T}'_{dis}$ and $\ddot{T}'_{dis}$ are performed by Kalman filter. Figure 26 shows the block diagram of force control using Kalman-filter-based force sensing with periodic component extraction. In this control scheme, a dither signal is inserted to the system to reduce friction effect of the ball-screw system. The DOB with conventional velocity estimation is used to estimate the oscillatory disturbance force caused by dither. The force estimation by Kalman filter is based on the oscillatory force estimated by DOB.

Here, we do not combine DOB and Kalman filter for high-order torque estimation, because using the Kalman filter as a state observer, we cannot determine the bandwidth of force sensing beforehand. Therefore, here, we apply the force estimation by DOB and the force estimation by Kalman filter serially. First, we determine the force sensing bandwidth of DOB to estimate the oscillatory torque. Then, the oscillatory torque will be used as an input to Kalman filter to estimate high-order oscillatory torques with noise suppression. Moreover, we do not use Kalman filter for velocity estimation because of the following reasons: Firstly, the velocity estimation by Kalman filter only reduces the noise in the velocity estimation. If it is used as the input of the DOB, the noise in the force estimation by DOB is reduced to a certain extent when the DOB pole is increased. However, here, we would like to estimate the high-order torque responses of the oscillatory torque estimated by DOB. The estimations of high-order torque are highly affected by noise when the DOB pole is increased. Therefore, using velocity estimation by Kalman filter will not have much effect on suppressing noise in high-order torque estimation. The high-order torque estimation with effective noise suppression is performed by Kalman filter. Secondly, we reduce the execution time of the controller by not using Kalman filter for velocity estimation.

In this method, we use RT-Linux instead of FPGA to implement the control algorithm with sampling time of 100 μs because it is very difficult to implement the whole control algorithm with the high-order estimations of Kalman filter in FPGA. It is impossible for us to implement this algorithm in FPGA. Moreover, for FPGA implementation, the calculations are usually based on fixed point numbers for reduction of FPGA resources and lower power consumption. However, the calculations based on fixed point have high quantization noise. On the other hand, the calculations in RT-Linux system are based on floating point numbers that have much less quantization noise than fixed point calculations. Hence, we implement the control algorithm with the high-order estimations of Kalman filter in RT-Linux to reduce the effect of calculation noise.

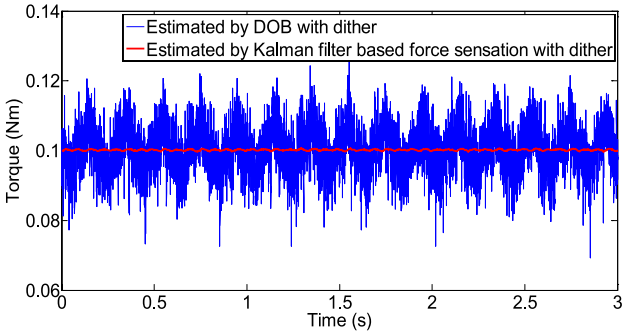

Fig. 27. Torque estimations at DOB pole of 1000 rad/s (5 Hz dither)

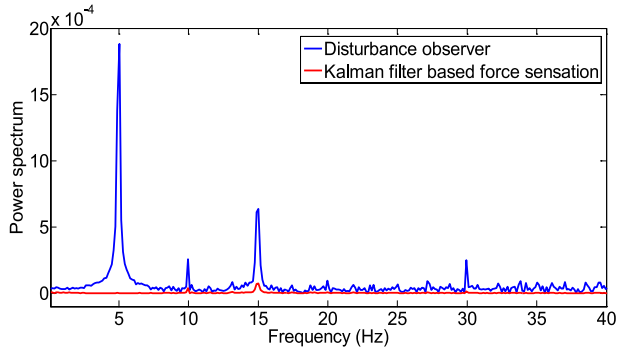

Fig. 28. FFT of torque responses in Fig. 27

The state, control input and observation matrices for Kalman filtering process are given as follows.

$$\boldsymbol{A} = \begin{bmatrix} 1 & T_s & 0 \\ 0 & 1 & T_s \\ 0 & -\omega_0^2 T_s & 1 - 2\zeta\omega_0 T_s \end{bmatrix}, \quad \boldsymbol{B} = \begin{bmatrix} 0 \\ 0 \\ 0 \end{bmatrix}, \quad \boldsymbol{H} = \begin{bmatrix} 1 & 0 & 0 \end{bmatrix}. \quad \cdots\cdots\cdots\cdots\cdots\cdots (50)$$

The estimated states by Kalman filter include T'_{dis}, $\dot{T}'_{dis}$ and $\ddot{T}'_{dis}$. $z_{(k)}$ is the periodical torque estimated by DOB, which is corrupted by noise. The estimated disturbance torque without oscillation component based on Kalman filter is applied to compute the compensation current to cancel the effects of the disturbance torque on the motor and the modeling errors. In this method, the effect of noise in the force estimation is suppressed effectively since the force sensation is based on estimations generated by the Kalman filter. Accordingly, it is possible to further widen bandwidth of force sensing by increasing the pole of DOB.

In order to evaluate the performance and verify the effectiveness of this method, the numerical simulation results based on the force-control experimental data of a ball-screw system are presented. The force-control experiment was carried out with a constant force command of 0.1 Nm. A 5 Hz-dither signal was inserted to the control reference signal. The

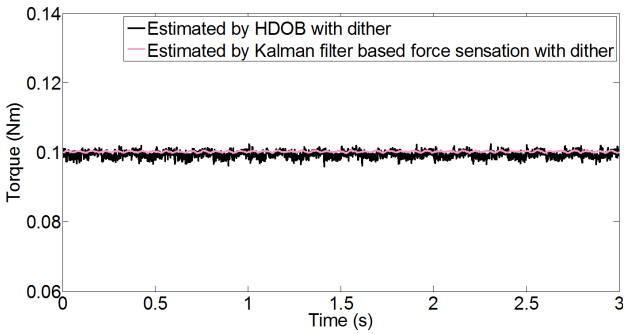

Fig. 29. Torque estimations by HDOB using Kalman filter and proposed method at force sensing bandwidth of 1000 rad/s in condition 5 Hz dither signal

DOB was used to estimate and compensate for disturbance torque. The experimental data of oscillatory torque T'_{dis} estimated by DOB were obtained during the force-control operation. In the experiments, the bandwidth of DOB is set to 1000 rad/s. These experimental data are used to perform the numerical simulation of the control scheme shown in Fig. 26. Figure 27 shows the torque estimation at force sensing bandwidth 1000 rad/s. The torque estimation by DOB is oscillatory and noisy while the Kalman-filter-based force estimation can eliminate the periodic component and suppress noise in torque estimation effectively. Figure 28 confirms the periodic component elimination of Kalman-filter-based method by FFT analysis. Figure 29 shows the torque estimations by HDOB using Kalman filter and the proposed method at force sensing bandwidth 1000 rad/s. The results show that the noise suppression performance of the proposed method is better than that of the HDOB using Kalman filter. These results confirm that the integration of force estimation by the DOB and the force estimation by Kalman filter constructs the force sensation with effective oscillatory component extraction and noise suppression. It is possible to further increase the bandwidth of the force sensation using the proposed method.

5. Conclusions

In this paper, a survey of motion control based on the Kalman filter and the DOB is presented. These control schemes have been proposed by the authors in previous works. Several control schemes as well as formulations and applications of the Kalman filter and the DOB are described in the paper. The performance and effectiveness of control schemes are evaluated through experimental results and numerical simulation results to provide a useful and comprehensive design of the Kalman filter and the DOB in various motion control applications.

References

(1) Y. Yokokura, S. Katsura, and K. Ohishi: "Stability analysis and experimental validation of a motion-copying system", *IEEE Trans. on Industrial Electronics*, Vol.56, No.10, pp.3906–3913 (2009)

(2) A. Sabanovic: "Challenges in motion control systems", *IEEJ Journal of IA*, Vol.6, No.2, pp.107–116 (2017)

(3) T. Tsuji, K. Ohnishi, and A. Sabanovic: "A controller design method based on functionality", *IEEE Trans. on Industrial Electronics*, Vol.54, No.6, pp.3335–3343 (2007)

(4) S. Khan, A. Sabanovic, and A.O. Nergiz: "Scaled bilateral teleoperation using discrete-time sliding-mode controller", *IEEE Trans. on Industrial Electronics*, Vol.56, No.9, pp.3609–3618 (2009)

(5) A. Hace, K. Jezernik, and A. Sabanovic: "SMC with disturbance observer for a linear belt drive", *IEEE Trans. on Industrial Electronics*, Vol.54, No.6, pp.3402–3412 (2007)

(6) K. Ohnishi: "Robust motion control by disturbance observer", *Journal of Robotics and Mechatronics*, Vol.8, No.3, pp.218–225 (1996)

(7) K. Ohnishi and K. Miyachi: "Torque-speed regulation of DC motor based on load torque estimation", *Proc. of IEEJ IPEC Tokyo*, Vol.2, pp.1209–1216 (1983)

(8) K. Ohnishi, M. Shibata, and T. Murakami: "Motion control for advanced mechatronics", *IEEE/ASME Trans. Mechatronics*, Vol.1, No.1, pp.56–67 (1996)

(9) Y. Xiong and M. Saif: "Unknown disturbance inputs estimation based on a state functional observer design", *Automatica*, Vol.39, No.8, pp.1389–1398 (2003)

(10) W.H. Chen, D.J. Balance, P.J. Gawthrop, and J. O'Reilly: "A nonlinear disturbance observer for robotic manipulators", *IEEE Trans. on Industrial Electronics*, Vol.47, No.4, pp.932–938 (2000)

(11) K. Natori, R. Oboe, and K. Ohnishi: "Stability analysis and practical design procedure of time delayed control systems with communication disturbance observer", *IEEE Trans. on Industrial Electronics*, Vol.4, No.3, pp.185–197 (2008)

(12) K.S. Kim, K.H. Rew, and S. Kim: "Disturbance observer for estimating higher order disturbances in time series expansion", *IEEE Trans. on Automatic Control*, Vol.55, No.8, pp.1905–1911 (2010)

(13) S. Oh and K. Kong: "High-precision robust force control of a series elastic actuator", *IEEE Trans. on Mechatronics*, Vol.22, No.2, pp.71–80 (2017)

(14) T.T. Phuong, C. Mitsantisuk, and K. Ohishi: "High performance force sensing based on Kalman-filter-based disturbance bbserver utilizing FPGA", *IEEJ Trans. IA*, Vol.131-D, No.3, pp.334–342 (2011)

(15) T.T. Phuong, K. Ohishi, Y. Yokokura, and C. Mitsantisuk: "FPGA-based high-performance force control system with friction-free and noise-free force observation", *IEEE Trans. on Industrial Electronics*, Vol.61, No.2, pp.994–1008 (2014)

(16) T.T. Phuong, K. Ohishi, and Y. Yokokura: "Motion-copying system using FPGA-based friction-free disturbance observer", *IEEJ Journal of IA*, Vol.3. No.3, pp.248–259 (2014)

(17) C. Mitsantisuk, S. Katsura, and K. Ohishi: "Kalman-filter-based sensor integration of variable power assist control based on human stiffness estimation", *IEEE Trans. on Industrial Electronics*, Vol.56, No.10, pp.3897–3905 (2009)

(18) C. Mitsantisuk, K. Ohishi, S. Urushihara, and S. Katsura: "Kalman filter-based disturbance observer and its applications to sensorless force control", *Journal of Advanced Robotics*, Vol.25, No.3-4, pp.335–353 (2011)

(19) C. Mitsantisuk, K. Ohishi, and S. Katsura: "Control of interaction force of twin direct-drive motor system using variable wire rope tension with multisensor integration", *IEEE Trans. on Industrial Electronics*, Vol.59, No.1, pp.498–510 (2012)

(20) C. Mitsantisuk, K. Ohishi, and S. Katsura: "Estimation of action/reaction forces for the bilateral control using Kalman filter", *IEEE Trans. on Industrial Electronics*, Vol.59. No.11, pp.4383–4393 (2012)

(21) T. Yoshioka, T.T. Phuong, A. Yabuki, K. Ohishi, T. Miyazaki, and Y. Yokokura: "High-performance load torque compensation of industrial robot using Kalman-filter-based instantaneous state observer", *IEEJ Journal of IA*, Vol.4, No.5, pp.589–590 (2015)

(22) T. Yoshioka, A. Yabuki, Y. Yokokura, K. Ohishi, T. Miyazaki, and T.T. Phuong: "Stable force control of industrial robot based on spring ratio and instantaneous state observer", *IEEJ Journal of IA*, Vol.5, No.2, pp.132–140 (2016)

(23) T.T. Phuong, K. Ohishi, Y. Yokokura, T.X. Bo, and A. Yabuki: "High performance load acceleration control based on singular spectrum analysis for industrial robot", *IEEE Proceedings of International Conference on Power Electronics and Motion Control (PEMC2016)*, pp.816–821, Varna, Bulgaria (2016)

(24) T.T. Phuong, K. Ohishi, and Y. Yokokura: "Kalman filter based fine force sensation with periodic component extraction", *IEEE Proceedings of 26th International Symposium on Industrial Electronics (ISIE2017)*, pp.1947–1952, Edinburgh, UK (2017)

(25) R. Oboe, R. Antonello, D. Pilastro, and K. Ito: "Use of MEMS inertial sensors for performance improvement of low-cost motion control systems", *IEEJ Journal of IA*, Vol.5, No.2, pp.78–89 (2016)

(26) R. Antonello, K. Ito, and R. Oboe: "Acceleration measurement drift rejection in motion control systems by augmented-state kinematic Kalman filter", *IEEE Trans. on Industrial Electronics*, Vol.63, No.3, pp.1953–1962 (2016)

(27) R.E. Kalman: "A new approach to linear filtering and prediction problems",

Journal of Basic Engineering, Transactions of the ASME, Vol.82, Series D, pp.35–45 (1960)
(28) S. Katsura, K. Ohnishi, and K. Ohishi: "Transmission of force sensation by environment quarrier based on multilateral control", *IEEE Trans. on Industrial Electronics*, Vol.54, No.2, pp.898–906 (2007)
(29) S. Katsura and K. Ohishi: "Acquisition and analysis of finger motions by skill preservation system", *IEEE Trans. on Industrial Electronics*, Vol.54, No.6, pp.3353–3361 (2007)
(30) K. Ogata: "Modern control engineering", 3rd Edition, Prentice Hall (1999)

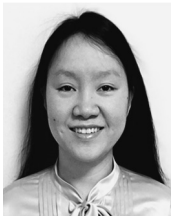

Thao Tran Phuong (Member) received B.S. degree in mechatronics engineering from University of Technical Education, Ho Chi Minh city, Viet Nam in 2007, M.S. degree in electrical, electronics and information engineering and Ph.D. degree in energy and environment science from Nagaoka University of Technology, Japan in 2010 and 2013, respectively. At present, she is a Postdoctoral researcher at Nagaoka University of Technology, Japan. Her interests include motion control, robotics, embedded systems, especially human support applications.

Kiyoshi Ohishi (Fellow) received the B.E., M.E., and Ph.D. degrees in electrical engineering from Keio University, Yokohama, Japan, in 1981, 1983, and 1986, respectively. From 1986 to 1993, Prof. Ohishi was an Associate Professor with Osaka Institute of Technology, Osaka, Japan. Since 1993, he has been with Nagaoka University of Technology, Nagaoka, Japan. He became a Professor in 2003 and a Vice President in 2015. His research interests include motion control, mechatronics, robotics and power electronics. He is a Fellow member of IEEE from 2015. He is a General chair of IEEE IECON2015. He is a General chair of IEEE AMC2010, AMC2016 and AMC2018. He is a Senior AdCom Member of IEEE IES Society from 2016, and he was an AdCom Member (elected) of IEEE IES Society for 12 years from 2004. He received the Outstanding Paper Awards at IECON'85 and Best Paper Awards at IECON'02, IECON'04 from the IEEE Industrial Electronics Society. He received twice "IEEJ Distinguished Paper Award" from IEEJ in 2002 and 2009, respectively.

Chowarit Mitsantisuk (Member) received the B.Eng. degree in electrical engineering from Thammasat University, Thailand, in 2004, and the M.Eng. degree in Electrical, Electronics and Information Engineering and D.Eng. degree in energy and environment science from the Nagaoka University of Technology, Japan, in 2007 and 2010, respectively. He was also a Postdoctoral Fellow of the Japan Society for the Promotion of Science. He joined the Kasetsart University, Thailand in 2012 as a lecturer and was promoted to assistant professor in 2015. Dr. Chowarit's research interests lie mainly in robot-created artwork, human-robot collaboration system, haptics, tele-operated robot, and rehabilitation robot. Dr. Chowarit is a Member of the IEEE Industrial Electronics Society. He was the recipient of the IEEE-IES Student Scholarship Award at the IECON'09, Best Paper Award at the iEECON'17 and ECTI-CON'17 and Best Presentation Award at IECON'12. His work on the human-robot collaboration system won the 2nd place in 2017 Robot Art world-wide competition.

Yuki Yokokura (Member) received the B.E. and M.E. degrees in electrical engineering from Nagaoka University of Technology, Niigata, Japan, in 2007 and 2009, respectively. In 2011, he received Ph.D. degree in integrated design engineering from Keio University, Yokohama, Japan. From 2010 to 2011, he was a JSPS (Japan Society for the Promotion of Science) Research Fellow (DC2 and PD). He was a Visiting Fellow at Keio University, and a Postdoctoral Fellow at Nagaoka University of Technology in 2011. Since 2012, he has been an Assistant Professor with Nagaoka University of Technology. His research interests include motion control, motor drive, power electronics, and real-world haptics.

Kouhei Ohnishi (Fellow) received the B.E., M.E. and Ph.D. in electrical engineering from the University of Tokyo in 1975, 1977 and 1980. Since 1980, he has been with Keio University. He served as a President of the IEEE Industrial Electronics Society in 2008 and 2009 as well as a President of IEEJ in 2015 and 2016. Since 2016, he has been also with KISTEC at Kawasaki, Japan. He received Purple Ribbon Medal Award from His Majesty the Emperor in 2016 and the IEEJ Meritorious Contribution Award in 2017.

Roberto Oboe (Member) was born in Lonigo, Italy, on October 26, 1963. He received the Laurea degree (cum laude) in electrical engineering and the Ph.D. degree from the University of Padova, Padova, Italy, in 1988 and 1992, respectively. He is presently Associate Professor of Automatic Control at the Department of Management and Engineering of the University of Padova, Vicenza, Italy. His research interests are in the fields of motion control, telerobotics, haptic devices, rehabilitation robots and applications and control of MEMS.

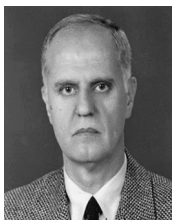

Asif Šabanovic (Non-member) Emeritus Professor, Sabanci University, Istanbul and International University, Sarajevo. He received B.S. degree in electrical engineering (in 1970), M.S. degree and Dr.Sci. degree from University of Sarajevo. Since 1970 till 1991 he has been with Energoinvest - Institute for Control and Computer Sciences, Sarajevo. From 1991till 2011he has been with University of Sarajevo, Department of Electrical Engineering. He has been Visiting Researcher at Institute of Control Science - Moscow (1975–1976). Visiting Professor at California Institute of Technology, Pasadena (1984–1985), Visiting Professor at Keio University, Yokohama (1991–1992), Full Professor at Yamaguchi University, Ube (1992–1993), Visiting Professor at University of Maribor- Maribor-Slovenia (Acad. Year 1986, 1988, 1989), Head of CAD/CAM and Robotics Department at Tubitak - Marmara Research Centre, Istanbul (1993–1995), Head of Engineering Department of B.H. Engineering and Consulting (1995–1999), Full professor at Sabancı University, Istanbul (1999–2015). He is a corresponding member of ANU BiH. His publications include 5 books, 2 edited books, 442 articles and conference papers. He received Best paper award, 2tth July award (the state award in Bosnia and Herzegovina). His fields of interest include Control Systems, Motion Control Systems, Robotics, Mechatronics and Power electronics.